Available online at www.sciencedirect.com
SCIENCE DIRECT®
Journal of Power Sources 141 (2005) 198–203
JOURNAL OF POWER SOURCES
www.elsevier.com/locate/jpowsour

Short communication

Preparation and characterization of composite electrodes of coconut-shell-based activated carbon and hydrous ruthenium oxide for supercapacitors

Mukta S. Dandekar, Girish Arabale, K. Vijayamohanan*

Physical and Materials Chemistry Division, National Chemical Laboratory, Pune 411008, India

Received 21 July 2004; accepted 16 September 2004
Available online 5 November 2004

Abstract

The relationship between the structure-specific capacitance ($F\,g^{-1}$) of a composite electrode consisting of activated coconut-shell carbon and hydrous ruthenium oxide ($RuO_x(OH)_y$) has been evaluated by impregnating various amounts of $RuO_x(OH)_y$ into activated carbon that is specially prepared with optimum pore-size distribution. The composite electrode shows an enhanced specific capacitance of $250\,F\,g^{-1}$ in 1 M H_2SO_4 with 9 wt.% ruthenium incorporated. Chemical and structural characterization of the composites reveals a homogeneous distribution of amorphous $RuO_x(OH)_y$ throughout the porous network of the activated carbon. Electrochemical characterization indicates an almost linear dependence of capacitance on the amount of ruthenium owing to its pseudocapacitive nature.

Keywords: Activated carbon; Composite; Supercapacitor; Specific capacitance; Pseudocapacitance; Electrochemical characterization

1. Introduction

Electrochemical capacitors (ECs) [1] are attractive energy-storage devices, particularly for applications that involve high-power requirements, such as electric vehicles (EVs) and hybrid EV systems [2]. The ECs boost the battery to provide the necessary power for acceleration, and additionally allow for recuperation of energy during regenerative braking. In addition, ECs are used as power sources for camera flash equipment, lasers and as back-up power sources for computer memory [3,4]. The energy-storage in a supercapacitor is achieved either by Faradaic or non-Faradaic processes at the electrode–electrolyte interface. Since the reversibility of the double-layer process at the surface of an electroactive material determines the capacitive performance, a high surface area is a key factor in achieving a high-capacitance.

Different types of specially-designed electrode materials have been intensely investigated in the past decade for fabricating supercapacitor electrodes. Some of the well-known materials include carbon nanotubes (CNT) [5–8], carbon aerogels [9], activated carbon [10–12], and conducting polymer-based nanocomposites [13,14]. Although CNTs are potential candidates for supercapacitors, commercial application is yet to be realized because of difficulties in mass production and purification. Furthermore, the properties of CNTs depend on their prehistory and hence their reproducibility is difficult with respect to their diameter and conductivity distribution. Carbon aerogels can also be used as electrode materials for supercapacitors, but the critical drying step involved in the synthesis of this material is hazardous and expensive for practical application. A comparison of these different materials shows that activated carbon is one of the most promising materials for fabricating supercapacitors, because of its low cost, inherent high surface area, structural stability, and electrochemical inertness within a wide potential window (up to 1 V in aqueous and 3.5 V in non-aqueous media) [15,16]. The specific capacitance of activated carbon is promoted by mixing it with various metal oxides, which causes a significant improvement in intra and inter-particle electronic

* Corresponding author. Tel.: +91 20 5893300; fax: +91 20 25893044.
E-mail address: viji@ems.ncl.res.in (K. Vijayamohanan).

0378-7753/$ – see front matter © 2004 Elsevier B.V. All rights reserved.
doi:10.1016/j.jpowsour.2004.09.008

conduction. The supercapacitive behaviour of several transition metal oxides, such as RuO_2, IrO_2, NiO_x and manganese oxide has already been evaluated [17–21]. Among these, hydrous ruthenium oxide $RuO_x(OH)_y$ has been recognized as one of the most promising candidates for electrodes as it can store charges by reversibly accepting and donating protons from an aqueous electrolyte. This process is governed by a potential-dependent equilibrium, as represented by:

$$RuO_x(OH)_y + \delta H^+ + \delta e^- \rightarrow RuO_{x-\delta}(OH)_{y+\delta} \quad (1)$$

$RuO_x(OH)_y$ is a mixed electronic–protonic conductor. Its electrochemical properties depend on the amount of water incorporated in its structure and the change of oxidation state (Ru^{4+}/Ru^{3+}) of ruthenium, which is responsible for the capacitance. Ruthenium is quite expensive as an electrode material for fabricating viable supercapacitors, and therefore a combination of $RuO_x(OH)_y$ with cheap activated carbon having a high surface area is a promising alternative, to other electrode materials such as CNT and carbon aerogels that are also expensive to produce. The present study examines the utility of activated (high surface area) carbon made from coconut-shell for composite electrodes for supercapacitors. The specific capacitance of this material is enhanced by preparing composites of the activated carbon with $RuO_x(OH)_y$ colloidal particles. The electrodes are characterized by various techniques, such as cyclic voltammetry, impedance analysis, X-ray diffraction (XRD), scanning electron microscopy (SEM) and pore-size analysis in conjunction with surface area measurements, to understand the reason for the capacitance increase.

2. Experimental

2.1. Sample preparation

A stable colloidal solution of $RuO_x(OH)_y$ was prepared by forced hydrolysis of a ruthenium chloride ($RuCl_3{\cdot}3H_2O$) precursor [22]. The composite samples were prepared by sonicating mixtures of activated carbon with different aliquots of the stable colloidal solution and distilled water in a 1:1 ratio for 2 h followed by mechanical stirring for 24 h. The sample was filtered and washed with distilled water until the pH was neutral to ensure that the solution was free of chloride ions. The samples were dried in air for 24 h at 110 °C, followed by annealing in air at 150 °C for 2 h.

2.2. Electrode fabrication

The electrodes were fabricated by mixing 75 wt.% sample with 20 wt.% graphite and 5 wt.% ethyl cellulose binder and the resultant mixture was pasted on to a stainless-steel mesh with the help of tetrahydrofuran solvent. The electrode was first compacted at room temperature, followed by hot-compaction at 155 °C for 2 min under a pressure of 1400 kPa. The electrodes were subsequently dried in a vacuum oven for 12 h to remove the adsorbed solvent.

2.3. Characterization

Electrochemical characterization was performed with a computer-controlled potentiostat/galvanostat (Autolab PGSTAT 30 with GPES software) using a three-electrode assembly in which the given composite electrode was used as the working electrode, $Hg|Hg_2SO_4$ as the reference electrode, and platinum foil as the counter electrode. Cyclic voltammetric measurements were carried out in the potential range of −0.8 to +0.7 V versus $Hg|Hg_2SO_4$ at different scan rates. Electrochemical impedance analysis was performed by an impedance analyzer (Autolab PGSTAT 30 with FRA software) in the frequency range 1 MHz to 0.1 Hz with an ac signal of 10 mV amplitude. All the electrochemical measurements were performed in 1 M H_2SO_4 electrolyte.

The XRD patterns of the samples were obtained on a Philips model 1730 X-ray diffractometer using Cu Kα ($\lambda = 1.5418$) radiation at 2θ values between 5 and 90°. A Leica stereoscan 440 model was used to examine the surface morphology of the samples by SEM, and the percentage of ruthenium was evaluated by the EDAX (energy dispersive analysis of X-rays) technique. A NOVA-1200 gas sorption analyzer was used to obtain N_2 adsorption–desorption isotherms. Barrett, Joyner and Halenda (BJH), *t*-plot methods were employed to determine the pore-size distribution and the total pore volume. The Brunauer–Emmett–Teller (BET) method was applied to measure the total surface area of each sample.

3. Results and discussion

3.1. X-Ray diffraction analysis (XRD)

A comparison of the XRD patterns of activated carbon and a typical composite containing 9 wt.% ruthenium hydroxide is presented in Fig. 1. Characteristic peaks appear at 2θ values of 24, 44 and 80° for the activated carbon and correspond to the (1 0 0), (1 1 1) and (3 0 0) planes, respectively. Although no discernible peaks are detected for the composite sample, the decrease in peak intensity on impregnating activated carbon with $RuO_x(OH)_y$ suggests that the latter material is in an amorphous state. The results are in excellent agreement with those reported by Kim and Popov. [23] and reveal that the $RuO_2{\cdot}xH_2O$ loaded on the Vulcan XC—72 substrate does not display any characteristic peaks when the composite samples are annealed at 150 °C and below, thus the RuO_2xH_2O is in the amorphous form. Interestingly, the composite sample annealed at 150 °C exhibits the highest capacitance, which confirms that $RuO_2{\cdot}xH_2O$ in the amorphous state is responsible for the increase in the specific capacitance of the substrate. When TiO_2 nanotubes were used as the substrate to load different amount of $RuO_2{\cdot}xH_2O$, [24], the XRD pat-

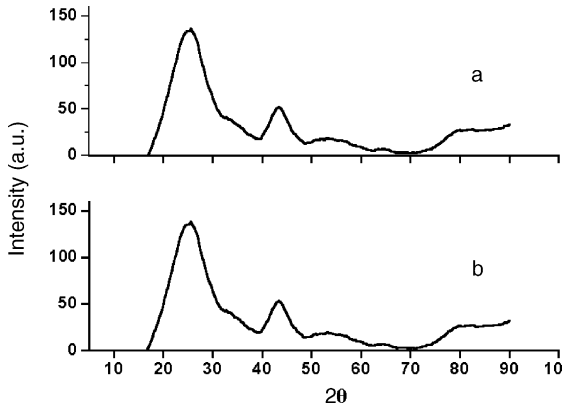

Fig. 1. Comparison of XRD pattern for (a) activated carbon and (b) composite with 9 wt.% ruthenium.

terns of the resulting composites indicated a decrease in the peak intensity of the TiO_2 nanotubes with no characteristic peaks for the $RuO_2{\cdot}xH_2O$ That finding also suggested that $RuO_2{\cdot}xH_2O$ was in the amorphous state and was responsible for the increase in specific capacitance. Thus, hydrous ruthenium oxide in the amorphous form is a prerequisite for high specific capacitance.

3.2. Structural characterization

Nitrogen gas adsorption–desorption studies can provide an alternative means for characterizing morphological changes in the composite samples. The variation of both specific surface area ($m^2\,g^{-1}$) and specific capacitance of the composite with various percentages of ruthenium is given in Fig. 2. Although activated carbon has a surface area of $1340\,m^2\,g^{-1}$, the composite shows only $460\,m^2\,g^{-1}$ after impregnation with 9 wt.% ruthenium. This decreasing trend is not surprising as several pores are likely to be filled by hydrous ruthenium oxide, as illustrated by the data listed in Table 1 that show the variation in surface area, pore area, pore volume and pore-size distribution in the activated carbon and the composite samples as a function of the amount of ruthenium. The initial increase in the average pore diameter from 18 to 21 Å can be attributed to blocking of some micropores by $RuO_x(OH)_y$. The surface area of these micropores contributes significantly to the total surface area and thus a decrease in the surface area is observed with increase in average pore diameter. Further decrease in the pore diameter to 17 Å suggests the blocking of some of the micropores as well as the mesopores of the activated carbon. A small increase in the surface area with the amount of ruthenium can be attributed to the presence of amorphous $RuO_x(OH)_y$ that is distributed homogeneously in the mesopores as well as in microporous region of the activated carbon. This is also in excellent agreement with the linear variation in specific capacitance as seen in Fig. 2; similar results have been reported by Miller and Dunn [25] who used a higher loading (60 wt.% ruthenium) of hydrous ruthenium oxide on carbon aerogel and obtained a specific capacitance of $270\,F\,g^{-1}$. By comparison, our results show $250\,F\,g^{-1}$ with only 9 wt.% ruthenium in the hydrous oxide. Hence, along with the amorphous hydrous ruthenium oxide, it is also necessary to choose a substrate with a high surface area and an optimum pore-size distribution for preparing composite electrodes for supercapacitors.

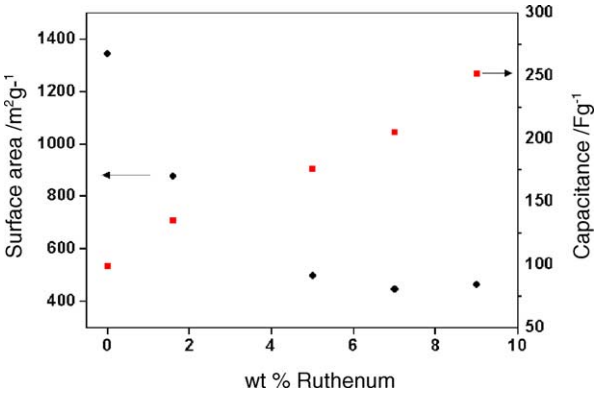

Fig. 2. Variation of surface area and specific capacitance with wt.% ruthenium in composite sample.

3.3. Scanning electron microscopy

Scanning electron micrographs reveal very small clusters of $RuO_x(OH)_y$ attached to large carbon granules in the composite samples (Fig. 3b), while activated carbon (Fig. 3a) consists of a smaller distribution of particles. Thus, there may be preferential nucleation sites for $RuO_x(OH)_y$ on the activated carbon surface. This is further confirmed by EDAX studies that show the presence of ruthenium on activated carbon with a peak around 2.50 kV. The percentage of ruthenium was calculated by averaging the values obtained from EDAX analysis at different positions on activated carbon.

3.4. Electrochemical characterization

Cyclic voltammograms for activated carbon and the composite sample in 1 M H_2SO_4 are presented in Figs. 4 and 5, respectively. The influence of scan rate on the specific capacitance, of the composite is given in Fig. 5(a); where the non-Faradaic current increases with increase in scan rate. For porous carbon electrodes, it is well-known that the higher the capacitance, the longer is the time required to acquire/release charges. Thus, the charge storage capability is increased at lower scan rate due to the influence of porosity on the RC time constant. The effect of cycling on the charge-storage capability of the composite electrode is presented in Fig. 5(b). The peak current increases with increase in the number of cycles and scan rate; the anodic peak shifts positively while the cathodic peak shifts negatively. The characteristic peaks that appear in the region −0.4 to +0.1 V are attributed to redox transitions such as Ru^{4+}/Ru^{3+} at the electrode–electrolyte interface in the $RuO_x(OH)_y$ according to Eq. (1). The specific

Table 1
Structural parameters of activated carbon and the composite samples

Amount of ruthenium (wt.%)	BET surface area ($m^2\ g^{-1}$)	Micropore area ($m^2\ g^{-1}$)	Mesopore area ($m^2\ g^{-1}$)	Micropore volume ($cm^3\ g^{-1}$)	Total pore volume ($cm^3\ g^{-1}$)	Average Pore diameter (Å)	Capacitance ($F\ g^{-1}$)
0	1340	1266	77.54	0.52	0.52	18	100
1.6	878	786.1	91.8	0.32	0.42	19	135
5	498	455.9	42.3	0.18	0.27	21	176
7	446	428.3	18.03	0.16	0.19	17	205
9	460	435.9	28.8	0.17	0.20	17	250

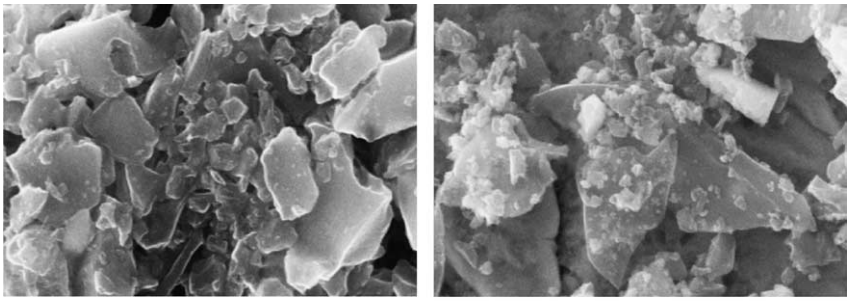

Fig. 3. Scanning electron micrograph of (a) activated carbon and (b) composite with 9 wt.% ruthenium.

capacitance of the activated carbon is significantly enhanced from 100 to 250 $F\ g^{-1}$ for the composite with 9 wt.% ruthenium in the hydrous oxide form. More interestingly, a linear relationship is observed between the specific capacitance and the amount of ruthenium impregnated into the activated carbon, as shown in Fig. 2. The present method has several advantages due to the formation of stable $RuO_x(OH)_y$, colloidal particles in the amorphous form to yield a high specific capacitance for a relatively low ruthenium loading compared with other reports [23,25], in which voltammograms have also been used to estimate specific capacitance. For example, Kim and Popov [23] found a specific capacitance in the range 220–280 $F\ g^{-1}$ for a 20 wt.% loading of ruthenium in the hydrous oxide form.

An electrochemical impedance technique has also been employed in order to understand the difference in the electrochemical behaviour between the activated carbon and composite electrodes. Typical complex plane plots for these electrodes are presented in Fig. 6. The double-layer charging, the charge-transfer resistance and the diffusion-controlled kinetics are all well-separated in the plots. The charge-transfer process at the electrode–electrolyte interface (Eq. (1)) is determined by the region represented by a semicircle at higher frequencies, whereas the straight line inclined at an angle of around 45° to the real axis represents the diffusion-controlled electrode kinetics in the lower frequency region. The frequency at which there is a deviation from the semicircle is the knee frequency, which reflects the maximum frequency at which capacitive behaviour is dominant. Comparison of the complex plane plot for activated carbon with that for the composite samples with varying percentages of ruthenium reveals some interesting differences. The diameter of the semicircle continues to increase with the increasing percentage of ruthenium. This clearly indicates that the resistance imposed by $RuO_x(OH)_y$ increases with the percentage of ruthenium in the composite sample. The straight line in the lower frequency region starts deviating from the behaviour exhibited by activated carbon as the pores are occupied by the amorphous $RuO_x(OH)_y$ in the various composite samples, as shown in Fig. 6. This, in turn, is reflected by the variation in structural parameters, such as surface area, mesopore area, and micropore area, as indicated in Table 1.

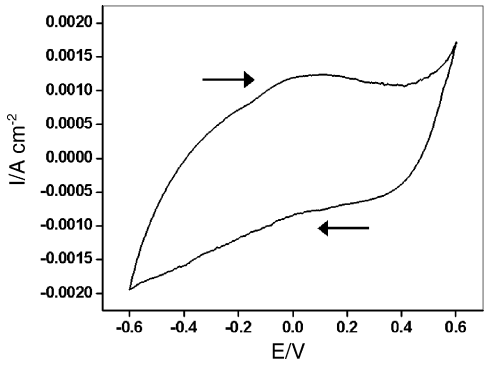

Fig. 4. Cyclic voltammogram of activated carbon at 1 mV s^{-1} in 1 M H_2SO_4. Arrow indicates direction of scan.

Various parameters such as the solution resistance (R_S, Ω), charge-transfer resistance (R_{CT}, Ω), and specific double-layer capacitance (C_{dl}, $F\ g^{-1}$) of the composite electrodes are given in Table 2 on the basis of commonly used Randles equivalent circuit. Though the values of specific capacitance are smaller than those calculated by the voltammetric techniques, there is a linear enhancement of specific capacitance. Thus, $RuO_x(OH)_y$ in the composite samples significantly increases the specific capacitance of activated carbon.

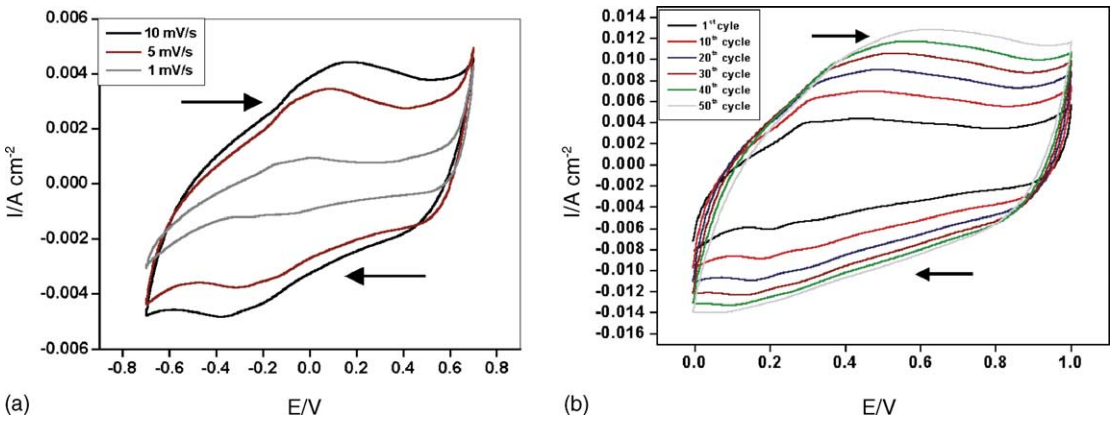

Fig. 5. (a) Cyclic voltammograms of composite sample at various scan rates (1, 5, 10 mV s^{-1}) in 1 M H_2SO_4 and (b) cyclic voltammograms of composite sample exhibiting cycle dependance of specific capacitance in 1 M H_2SO_4.

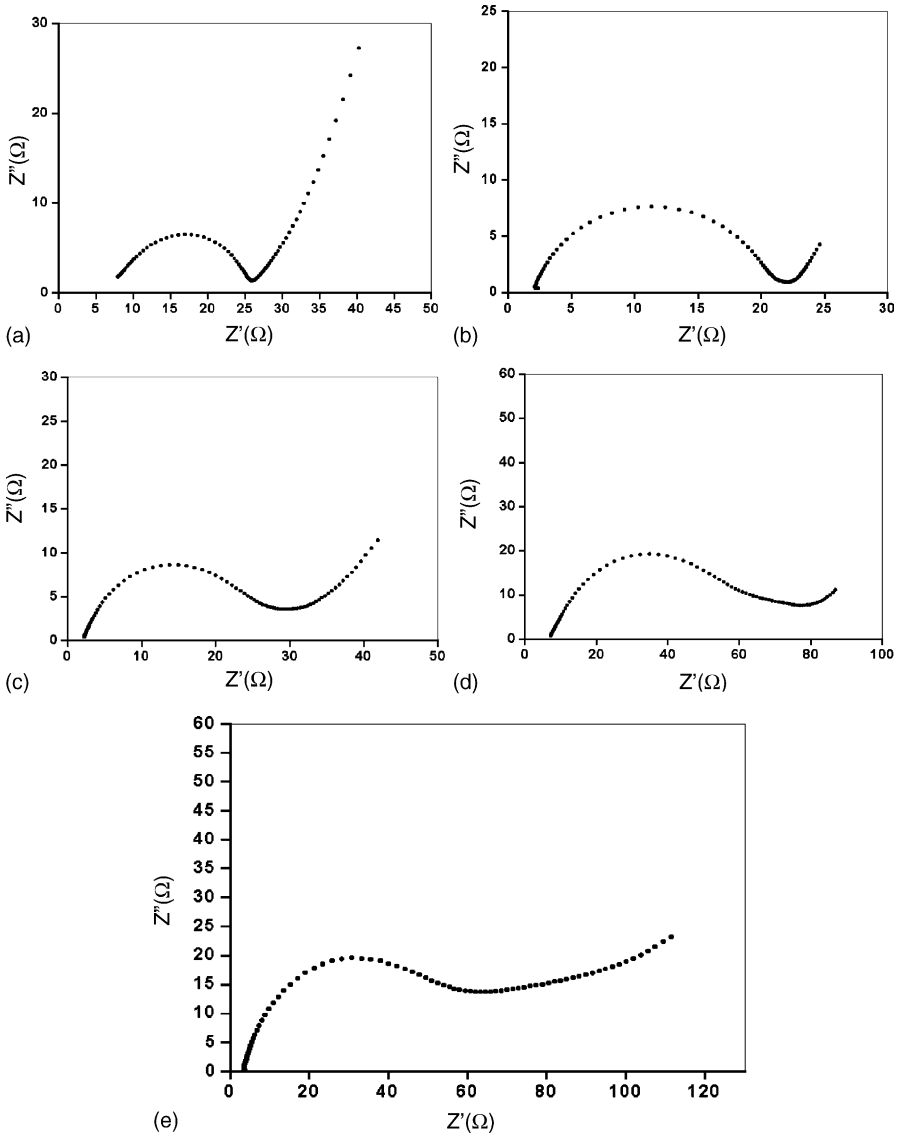

Fig. 6. Complex plane plots for (a) activated carbon and composites in 1 M H_2SO_4. Amount of $RuO_2{\cdot}xH_2O$ in composites is (b) 1.6 wt.%, (c) 5 wt.%, (d) 7 wt.% and (e) 9 wt.%.

Table 2
Parameters calculated from impedance analysis

Amount of ruthenium (wt.%)	R_S (Ω)	R_{CT} (Ω)	C_{dl} (mF g^{-1})
0	7.5	26.3	3.44
1.6	2.2	20.8	20.10
5	2	27.6	50.31
7	2.5	62	59.33
9	2	65	62.83

4. Conclusions

The impregnation of $RuO_x(OH)_y$ has been found to be an effective method for improving the energy-storage capabilities of activated (high surface area) carbon. The impregnation process results in a composite material with homogeneously dispersed $RuO_x(OH)_y$ colloidal particles throughout the porous network of the activated carbon. The presence of ruthenium in the activated carbon is confirmed by SEM and EDAX, while XRD studies reveal that $RuO_x(OH)_y$ is in an amorphous state, which is responsible for the significant increase in the specific capacitance. Cyclic voltammetric studies reveal an increase in the specific capacitance of the activated carbon from 100 to 250 F g^{-1} for the composite with 9 wt.% ruthenium. Electrochemical impedance analysis suggests that the energy-storage process of these composite materials, as well as that of pure activated carbon, is limited by the mass transport of electrolyte ions in the pores of the activated carbon. This type of composite material containing a small amount of amorphous hydrous ruthenium oxide is a promising candidate for supercapacitor electrodes.

Acknowledgement

The authors are grateful to the Ministry of Non-Conventional Energy Sources (MNES), Delhi, India, for the financial support given to conduct this study.

References

[1] B.E. Conway, Electrochemical supercapacitors—Scientific Fundamentals and Technological Applications, Kluwer Academic Publisher, Plenum Press, Dordrecht, New York, USA, 1999.
[2] R. Kotz, M. Carlen, Electrochim. Acta 45 (2000) 2483–2498.
[3] C.-C. Wang, C.-C. Hu, Mater. Chem. Phys. 83 (2004) 289–297.
[4] P.V. Adhyapak, T. Maddanimath, S. Pethkar, A.J. Chandwadkar, Y.S. Negi, K. Vijayamohanan, J. Power Sources 109 (2002) 105–110.
[5] G. Arabale, D. Wagh, M. Kulkarni, I.S. Mulla, S.P. Vernekar, K. Vijayamohanan, A.M. Rao, Chem. Phys. Lett. 376 (2003) 207–213.
[6] X. Qun, S. Durbach, G.T. Wu, Carbon 42 (2004) 451–453.
[7] E. Frackowaik, F. Beguin, Carbon 40 (2002) 1775–1787.
[8] Ch. Emmenegger, Ph. Mauron, P. Sudan, P. Wenger, V. Hermann, R. Gallay, A. Zuttel, J. Power Sources 124 (2003) 321–329.
[9] H. Probstle, C. Schmitt, J. Fricke, J. Power Sources 105 (2002) 189–194.
[10] K. Kierzek, E. Frackowiak, G. Lota, G. Gryglewicz, J. Machnikowaski, Electrochim. Acta 49 (2004) 515–523.
[11] E. Frackowaik, F. Beguin, Carbon 39 (2001) 937–950.
[12] D. Qu, J. Power Sources 4794 (2002) 1–9.
[13] Q. Xiao, X. Zhou, Electrochim. Acta 48 (2003) 575–580.
[14] W.-C. Chen, T.C. Wen, H. Teng, Electrochim. Acta 48 (2003) 641–649.
[15] H. Liang, F. Chen, R. Li, L. Wang, Z. Deng, Electrochim. Acta 49 (2004) 3463–3467.
[16] C.-C. Hu, C.-C. Hu, J. Power Sources 125 (2004) 299–308.
[17] W. Chen, C. Hu, C. Wang, C. Min, J. Power Sources 125 (2004) 292–298.
[18] V. Horvat-Radosevic, K. Kvastek, M. Vukovic, D. Cukman, J. Electroanal. Chem. 482 (2000) 188–201.
[19] C. Hu, K. Chang, J. Power Sources 4936 (2002) 1–9.
[20] F. Zhang, Y. Zhou, H. Li, Mater. Chem. Phys. 83 (2004) 260–264.
[21] M. Wu, G.A. Snook, G.Z. Chen, D.J. Fray, Electrochim. Commun. 6 (2004) 499–504.
[22] V. Panic, T. Vidakovic, S. Gojkovic, A. Dekanski, S. Malonjic, B. Nikolic, Electrochim. Acta 48 (2003) 3805–3813.
[23] H. Kim, B.N. Popov, J. Power Sources 104 (2002) 52–61.
[24] W. Yong-gang, Z. Xiao-Gang, Electrochim. Acta 49 (2004) 1957–1962.
[25] J.M. Miller, B. Dunn, Langmuir 15 (1999) 799–806.